IEEE Access
Multidisciplinary ⋮ Rapid Review ⋮ Open Access Journal

Received December 27, 2018, accepted January 12, 2019, date of publication January 18, 2019, date of current version February 8, 2019.

Digital Object Identifier 10.1109/ACCESS.2019.2893403

Performance Analysis for User-Centric Dense Networks With mmWave

JIANFENG SHI[1], (Student Member, IEEE), CUNHUA PAN[2], (Member, IEEE), WENCE ZHANG[1,3,4], (Member, IEEE), AND MING CHEN[1], (Member, IEEE)

[1]National Mobile Communications Research Laboratory, Southeast University, Nanjing 210096, China
[2]School of Electronic Engineering and Computer Science, Queen Mary University of London, London E1 4NS, U.K.
[3]School of Computer Science and Telecommunication Engineering, Jiangsu University, Zhenjiang 212000, China
[4]NCRL, Southeast University, Nanjing 210096, China

Corresponding author: Jianfeng Shi (shijianfeng@seu.edu.cn)

This work was supported in part by the National Science and Technology Major Project under Grant 2016ZX03001016-003, in part by the National Natural Science Foundation of China under Grant 61871128, Grant 61372106, and Grant 61221002, in part by the Nature Science Foundation of Jiangsu Province under Grant BK20170557, in part by the Nature Science Foundation for Higher Education Institutions of Jiangsu Province of China under Grant 17KJB510009, and in part by the Open Research Fund of the National Mobile Communications Research Laboratory, Southeast University, under Grant 2018D13.

ABSTRACT This paper focuses on the coverage probability and ergodic capacity for millimeter wave (mmWave) user-centric dense networks, where multiple access points (APs) consist of a virtual cell for each user equipment and transmit data with mmWave antennas cooperatively. All APs are distributed according to a homogeneous Poisson point process. Different from the low-frequency band (below 3 GHz), blockages have a non-negligible effect on mmWave band. To illustrate the effect, we utilize a line-of-sight probability function, which is dependent on the link-length. Then, via stochastic geometry, the expressions for coverage probability and ergodic capacity are derived, which accounts for: blockages, different small-scale fading distributions (Nakagami, Rayleigh, and no fading), and AP cooperation. In addition, we deduce the approximate expressions for coverage probability and ergodic capacity by using the noise-limited approximation. The numerical results validate our analytical expressions and show that the AP cooperation can provide high coverage performance and distinct capacity gain in a lower-AP-density region.

INDEX TERMS User-centric dense networks, millimeter wave, Poisson point process, ergodic capacity, coverage probability.

I. INTRODUCTION

According to [1], mobile data traffic has grown 18-fold over the past 5 years and will exceed half a zettabyte by 2021. In addition, the number of mobile-connected devices per capita will reach 1.5 by 2021. Thus, to meet these requirements, user-centric virtual cell (VC) networks have been proposed in [2] as one of five key breakthrough technologies for the fifth generation (5G) systems, since it can offer ubiquitous user experience and provide remarkable improvements in both spectral efficiency (SE) and energy efficiency (EE). Note that the user-centric VC network was first proposed as a novel concept in [3], where a VC was composed with a user equipment (UE) at the cell center and its serving access points (APs) located in a circular area. Specifically, there are three components in a user-centric VC network, i.e., UE, AP, and the central controller. many APs are distributed over the coverage area and connected to a central controller via high-speed dedicated links. Each UE is served by its surrounding APs collaboratively. Compared with conventional AP-centric cells, the user-centric VC network possesses tremendous advantages [3], [4] (e.g., elimination of cell-edge problem, capacity enhancement due to cooperation, lessened performance dependency on the users' positions).

On the other hand, since the current spectrum (300 MHz-3 GHz) is scarce, it is vital to exploit the huge segment of the millimeter wave (mmWave) spectrum band [5]. As a result, the mmWave communications have been attracted more and more attention in both academia and industry. Furthermore, mobile operators and network vendors have to investigate the dense networks to tackle the 1000×Data Challenge [6], which are expected to operate in the mmWave spectrum band [7]. From the perspective of mmWave communication, it is also of importance for relieving the signal interception to deploy APs densely due to the blockage sensitivity [8].

In this work, we incorporate the above three key enablers (user-centric VC network, dense network and mmWave communication) into one framework, which make the unified network be a desirable candidate for the next generation communication systems. To be more specific, in user-centric VC dense networks, the massive deployment of APs renders the short-range mmWave technologies (operating in 30-300 GHz) very promising [9] and can achieve better system performance in terms of the coverage and rate [10]. Moreover, with dense deployment, the networks can boost the unprecedented capacity and realize the exceptionally demanding mission-critical and resource-hungry applications [11]. Meanwhile, the AP cooperation can further increase the SE and EE. Thus, in such a user-centric VC dense network, we derive the key performance metrics by using the stochastic geometry.

A. PREVIOUS WORKS

The performance for user-centric networks with conventional low-frequency was extensively studied in [12]–[16], where the expressions for the outage probability, coverage probability, SE, EE, and ergodic rate were deduced. Specifically, closed-form expressions of the coverage probability, SE and EE were derived in [12], where the locations of APs are modeled as a marked Poisson point process (PPP). An explicit expression for the successful access probability (SAP) was derived in [13], where SAP is defined as a conditional probability of signal-to-noise-and-interference ratio (SINR) is greater than a threshold, given the condition that the serving AP cluster is determined. To acquire accurate analytical results of outage probability and ergodic rate, the Gauss-Chebyshev integration was applied in [14], where all APs are uniformly distributed inside a disk. By employing the multi-antenna technology, an exact closed-form expression for the outage probability was derived for the given selection transmission scheme in single user downlink multiple-input single-output (MISO) network [15]. In addition, analytical approximations of the outage probability were derived for other two transmission schemes (e.g., all the APs participate and the minimal number of APs participate), which are tight at high signal-to-noise ratio (SNR). With a similar system assumption to [15], an accurate uplink closed-form ergodic capacity expression was derived in [16].

Different from the low-frequency band, mmWave communications suffer from severe path loss and possess the feature of significant directionality [17]. Thus, the analytical results and methods in [12]–[16] cannot be applied directly in our work.

The coverage and rate performance of mmWave cellular networks were studied in [18]–[23]. Specifically, an exact integral expression for the coverage probability and average achievable rate were obtained in [18] by adopting the noise-limited approximation (i.e., SINR $\approx$ SNR), which is tight for typical AP density. Bai and Heath [19] proposed the tractable and general models to characterize the coverage and rate performance. The expressions for the coverage probability and achievable rate were expressed as a function of the antenna geometry and base station density. In addition, a more efficient approach was provided to calculate the expressions by avoiding inverse Fourier Transform. The expressions for coverage and rate performance were also derived in [20] and by incorporating self-backhauling in [21].

However, the above-mentioned works [18]–[21] did not consider the effect of AP cooperation, which will make the analysis intractable. Thus, the results in these works cannot be extended to our paper, since we consider the AP cooperation in the analysis. Although Maamari *et al.* [22] and He *et al.* [23] studied the performance with AP cooperation, they ignored some important terms (e.g., small-scale fading coefficient and inter-user interference). To be more specific, the expressions for coverage probabilities in the downlink of mmWave heterogeneous networks were derived in [22], where the authors assumed a special case, i.e., always Rayleigh fading on the interference links. In mmWave cloud radio access networks (CRANs), [23] analyzed the outage performance as an opposite of coverage performance, where the expressions for the outage probability were derived by ignoring small-scale fading term and interference power.

B. MOTIVATION AND MAIN CONTRIBUTIONS

To the best of our knowledge, performances for user-centric VC dense networks with mmWave have not been analyzed widely, since these networks contain many crucial factors (e.g., AP cooperation, sharp directionality, blockage sensitivity, severe path loss, etc.). Although the previous works had the limitations of their own and did not analyze the performance metrics in such networks, they are quite inspiring for our paper. Specifically, inspired by [19] and [22], we study the coverage probability and ergodic capacity for a downlink VC dense networks with mmWave in this paper.

However, different from [19], we study the coverage probability and ergodic capacity involving AP cooperation. Although the AP cooperation is straightforward, it is intractable to obtain the distribution of desired power. Thus, it is more difficult to derive the coverage probability than that in [19], since [19, Lemma 6] cannot be applied in our paper, which is a key step to derive the coverage probability. To tackle with this difficulty, we analyze the coverage probability through a different method in our paper. Compared with [22], we adopt the K-nearest AP association strategy in our paper, i.e., a typical UE chooses the K-closest APs to form its VC. Specifically, Maamari *et al.* [22] considered a multi-tier heterogeneous network, thus the set of cooperating APs is chosen based on the K-best AP association method from different tiers. However, in our paper, the set of cooperating APs is formed by the closest ones from the same tier. Although the coverage probability was also derived in Maamari *et al.* [22] assumed a special case, i.e., always Rayleigh fading on the interference links. However, in our paper, we investigate the performance by considering general cases, i.e., different small-scale fading both on the desired and interference links, which is more difficult to analyze.

In summary, the main contributions of this paper are presented as follows:

1) Considering three different small-scale fading distribution (i.e., Nakagami, Rayleigh and no fading), integral expressions for the ergodic capacity and coverage probability are derived for the typical UE. Specifically, the detailed derivations take into account the AP location randomness, blockage-dependent path loss, small-scale fading, directional antenna gain and the AP cooperation. To make it tractable, we propose a strong but reasonable assumption (i.e., the serving APs are assumed to be in LOS with dense deployment), which is verified by the simulation results.
2) Recent works [17] and [21] indicate that mmWave communications tend to be more noise-limited than the low-frequency networks. Thus, to exploit the noise-limited feature of mmWave communications, we deduce the approximate expressions for the ergodic capacity and coverage probability through using the noise-limited approximation.
3) Numerical results first show that the probability of the serving APs being in LOS increases with density and tends to be 1, which is also affected by the number of serving APs and radius of considered region. Then, numerical results indicate that our analytical expressions match well with the simulation results and the AP cooperation can provide high coverage performance and distinct capacity gain under various simulation parameters. Moreover, the noise-limited characteristic of mmWave communications is closely related to the AP density.

C. ORGANIZATION

In Section II, we present the system model, including network model, path loss model, directional antenna model and SINR model. Section III analyzes the coverage probability and ergodic capacity under three small-scale fading distribution, respectively. Numerical results and the corresponding discussions are given in Section IV. Finally, we conclude this paper in Section V.

II. SYSTEM MODEL

A. NETWORK MODEL

Consider a downlink user-centric virtual cell (VC) dense network where a typical UE is located at the origin[1] and all the mmWave APs are deployed according to a homogeneous Poisson Point Process (PPP) Φ with density λ. Each AP is connected to a central controller via high-speed dedicated links (e.g., fiber optics). The UE is assumed to select the K-closest APs to form its VC, as shown in Fig. 1.

[1]When the UEs are distributed as an independent stationary point process, the characteristics of coverage probability and ergodic capacity at the typical UE are identical to the other UEs in the network [19], [24]. Thus, in this paper, we consider a typical UE located at the origin.

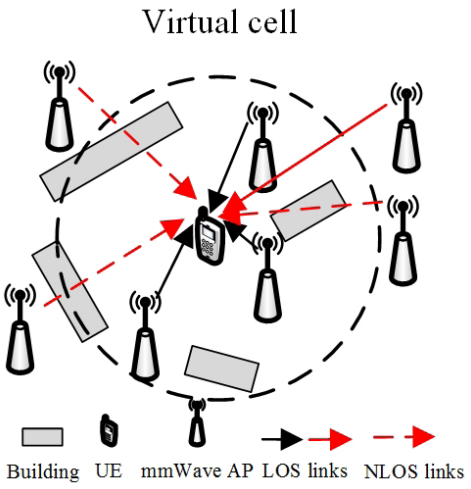

FIGURE 1. A scenario of the downlink virtual cell networks where $K = 3$. The black and red links mean the useful and interference links, respectively.

Generally, the K-nearest[2] AP association strategy is adapted to form a VC in user-centric networks [16], [25], which is more practical than the K-best AP strategy (i.e., the K APs with maximal received power) due to less backhaul signaling overhead. Let $\mathcal{V}_0$ be the set of serving APs. All APs share the same resource to transmit data. Thus, the UE suffers the interference from the APs not belonging to $\mathcal{V}_0$. Denote the Euclidean distance between the kth AP and the typical UE by r_k. Without loss of generality, we assume that $r_1 < r_2 < \cdots < r_K$. Because of the blockage effect, an AP can be either LOS or NLOS to the UE, as illustrated in Fig. 1. However, with dense deployment, it is reasonable to assume that the link between any serving AP to the UE is LOS.[3]

B. TRANSMISSION MODEL

1) PATH LOSS

For mmWave communication, path loss model is different from that operating under the low-frequency band, which is closely related to the effect of blockage. Based on [26], we assume that the blockages are modeled as a rectangle Boolean scheme. Specifically, denote the LOS probability function by $p(r)$, which represents the probability that a link with length r is LOS. Accordingly, the probability of a NLOS link is $1 - p(r)$. Then, $p(r) = e^{-\beta r}$, where β is a parameter dependent on the features of blockages. Given a link-length r, the path loss function $L(r)$ is given by

$$L(r) = \begin{cases} C_L r^{-\alpha_L}, & \text{with probability } p(r) \\ C_N r^{-\alpha_N}, & \text{with probability } 1 - p(r), \end{cases} \tag{1}$$

where, α_L (α_N) and C_L (C_N) are the path loss exponents and coefficients of the LOS (NLOS) link.

[2]How to determine the numerical value of K is a crucial issue for user-centric networks, while it is beyond the scope of this paper.

[3]This assumption will be verified by the simulation results in Section IV.

2) SMALL-SCALE FADING

Denote the small-scale fading coefficient on the kth link by ξ_k. In this paper, we consider three small-scale fading distributions. Firstly, in the case that the fading is Nakagami distributed, $|\xi_k|^2$ is a normalized Gamma random variable (r.v.) with $|\xi_k|^2 \sim \Gamma(N_L, 1/N_L)$ when the kth link is LOS and $|\xi_k|^2 \sim \Gamma(N_N, 1/N_N)$ when it is NLOS [19]. Here, N_L and N_N are the Nakagami parameters for LOS and NLOS links, respectively. Secondly, under the Rayleigh fading distribution, ξ_k is modeled as a zero mean complex Gaussian r.v. and $|\xi_k|^2 \sim \exp(\mu)$, where μ is the parameter of the exponential distribution. Thirdly, without small-scale fading, we ignore ξ_k by letting $|\xi_k|^2 = 1$ in the corresponding formulas.

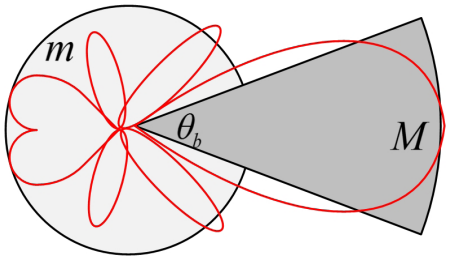

FIGURE 2. Approximate sectored antenna model of mmWave communication. The actual model consisted of the red line is approximated by the sector region consisted of the black line.

3) ANTENNA MODEL

we assume that all APs are equipped with directional antennas, which approximatively follow a sectored antenna model, shown in Fig. 2. The beam-width is denoted by θ_b. Then the antenna gain for a mmWave AP can be written as a function of angle θ about steering angle [21], given by

$$A_b(\theta) = \begin{cases} M, & \text{if } \theta < \theta_b \\ m, & \text{otherwise.} \end{cases}$$

The antenna gain $A_u(\theta)$ at the UE terminal can be modeled in the same manner, whereas we assume that the omni-directional antenna[4] is adopted at the UE for simplicity, i.e., $A_u(\theta) = 1$.

We assume that the serving APs transmit to the typical UE with the maximum antenna gains via beam alignment. Let us denote G_k as the antenna gain from the kth AP to UE. Then, $G_k = M, \forall k \in \mathcal{V}_0$. Furthermore, for the interference links, we assume that the interfering APs' angles are distributed independently and uniformly in $(0, 2\pi]$. As a result, the antenna gain of the interfering APs $G_l, \forall l \notin \mathcal{V}_0$ is a discrete r.v.. Its probability distribution function is given by $\mathbb{P}(G_l = a_n) = b_n$, $n = 1, 2$, where $\mathbb{P}(\cdot)$ means the probability of an event, $a_1 = M$, $b_1 = \theta_b/2\pi$, $a_2 = m$ and $b_2 = 1 - \theta_b/2\pi$.

[4]If the directional antenna is equipped at the UE, one needs to consider the beam alignment problem, which is interesting and left for future research.

4) SINR EXPRESSION

We assume that all APs transmit with the same power P_t. Then, the SINR at the typical UE can be expressed as [27]

$$\gamma = \frac{P}{P^{(I)} + \sigma^2} = \frac{\sum_{k\in\mathcal{V}_0} G_k L(r_k)|\xi_k|^2}{\sum_{l\notin\mathcal{V}_0} G_l L(r_l)|\xi_l|^2 + \sigma^2}, \quad (2)$$

where P is the desired signal power of the typical UE, $P^{(I)}$ is the interference power from other APs, and σ^2 is the thermal noise power normalized by the transmitting power P_t. It is worth noting that the SINR in (2) is a r.v., because of the randomness in the antenna gain G_l, path loss function $L(r)$, distance r_l and small-scale fading ξ_l.

III. PERFORMANCE ANALYSIS

In this section, we first provide the mathematical preliminaries and then derive the coverage probability and ergodic capacity under three small-scale fading distributions (i.e., Nakagami, Rayleigh and no fading).

A. PRELIMINARIES

Due to the blockage, only a subset of the interfering APs is in LOS. Denote the point process of the LOS and NLOS APs by Φ_L and Φ_N, respectively. With negligible accuracy loss, Φ_L and Φ_N can be modeled as two independent non-homogeneous PPP with the density function $\lambda p(r)$ and $\lambda(1 - p(r))$, respectively [19]. Then, the SINR can be reformulated as

$$\gamma = \frac{\sum_{k\in\Phi\cap\mathcal{B}(0,r_K)} MC_L r_k^{-\alpha_L}|\xi_k|^2}{I_L + I_N + \sigma^2}, \quad (3)$$

where $\mathcal{B}(0, r_K)$ denotes the ball centered at the origin of radii r_K, $I_L = \sum_{l\in\Phi_L\cap\bar{\mathcal{B}}(0,r_K)} G_l C_L r_l^{-\alpha_L}|\xi_l|^2$, $I_N = \sum_{l\in\Phi_N\cap\bar{\mathcal{B}}(0,r_K)} G_l C_N r_l^{-\alpha_N}|\xi_l|^2$ are the interference power from the LOS and NLOS APs,[5] $\bar{\mathcal{B}}(0, r_K)$ represents the region outside $\mathcal{B}(0, r_K)$.

The coverage probability of typical UE is defined as

$$\Pr \triangleq \mathbb{P}(\gamma > \gamma_{th}), \quad (4)$$

where γ_{th} is the predetermined SINR threshold. The ergodic capacity (bps/Hz) of typical UE is given by

$$C \triangleq \mathbb{E}_{\mathbf{G},\mathbf{r},\boldsymbol{\xi}}[\log_2(1 + \gamma)], \quad (5)$$

where $\mathbf{G} = \{G_l, \forall l\}$, $\mathbf{r} = \{r_l, \forall l\}$, $\boldsymbol{\xi} = \{\xi_l, \forall l\}$, and $\mathbb{E}[\cdot]$ stands for the mathematical expectation. Given the condition that the serving APs of the typical UE are at distances of $r_1, \cdots, r_K$, the ergodic capacity can be rewritten as

$$C = \int \cdots \int_{\mathcal{D}} C_{\text{cond}} f_{r_1,\cdots,r_K}(r_1, \cdots, r_K)\mathrm{d}\boldsymbol{r}, \quad (6)$$

where the multiple integral domain is $\mathcal{D} = \{0 < r_1 \leqslant \cdots \leqslant r_K\}$, $\mathrm{d}\boldsymbol{r} = \mathrm{d}r_1 \cdots \mathrm{d}r_K$, C_{cond} is the conditional

[5]Note that the interference power can be divided into LOS and NLOS parts, due to the effect of blockage.

ergodic capacity, given the condition that $r_1 \leqslant \cdots \leqslant r_k \leqslant \cdots \leqslant r_K, k \in \mathcal{V}_0$. $f_{r_1,\cdots,r_K}(r_1,\cdots,r_K)$ is the joint probability density function (PDF) of $r_1,\cdots,r_K$, given by [28, eq. (30)]

$$f_{r_1,\cdots,r_K}(r_1,\cdots,r_K) = (2\pi\lambda)^K r_1 \cdots r_K e^{-\pi\lambda r_K^2}. \quad (7)$$

B. COVERAGE PROBABILITY AND ERGODIC CAPACITY WITH NAKAGAMI FADING

In this subsection, we analyze the coverage probability and ergodic capacity when the small-scale fading is Nakagami fading. As mentioned before, if the lth link is LOS (or NLOS), $|\xi_l|^2$ is a normalized Gamma r.v. with shape parameter N_L (or N_N) and scale parameter $1/N_L$ (or $1/N_N$). Since a closed form expression for the distribution of P cannot be obtained (except for the case of $K = 1$), we derive the coverage probability in Theorem 1 relying on the coverage probability for a general fading distribution [29, Proposition 2.2]. Then, the ergodic capacity for user-centric dense networks is given in Theorem 3.

In addition, to exploit the noise-limited characteristic of mmWave communication, we further deduce the coverage probability and ergodic capacity via the noise-limited approximation (i.e., SINR $\approx$ SNR). The approximate expressions for coverage probability and ergodic capacity with Nakagami fading are given in Corollary 2 and 4, respectively.

Theorem 1: An expression for coverage probability with Nakagami fading is given by

$$\Pr = \int\cdots\int_{\mathcal{D}} (2\pi\lambda)^K r_1\cdots r_K e^{-\pi\lambda r_K^2} \int_{-\infty}^{\infty} e^{-2\pi j\gamma_{th}s\sigma^2} \times e^{-Q_L(2\pi j\gamma_{th}s)} e^{-Q_N(2\pi j\gamma_{th}s)} \frac{\mathcal{L}_P(-2\pi js)-1}{2\pi js} \mathrm{d}s\mathrm{d}r, \quad (8)$$

where

$$Q_L(s) = \sum_{n=1}^{2} 2\pi\lambda b_n \int_{r_K}^{\infty} F(N_L, sa_nC_Lx^{-\alpha_L}) p(x) x \mathrm{d}x, \quad (9)$$

$$Q_N(s) = \sum_{n=1}^{2} 2\pi\lambda b_n \int_{r_K}^{\infty} F(N_N, sa_nC_Nx^{-\alpha_N})(1-p(x)) x \mathrm{d}x, \quad (10)$$

$$\mathcal{L}_P(s) = \prod_{k=1}^{K} (1 - F(N_L, sMC_Lr_k^{-\alpha_L})), \quad (11)$$

$F(N,x) = 1 - 1/(1+x/N)^N$, a_n *and* b_n *are defined in Subsection II-B.*

Proof: The proof is given in Appendix A. □

Corollary 2: The approximate coverage probability in noise-limited scenarios with Nakagami fading can be written as

$$\widetilde{\Pr} = \int\cdots\int_{\mathcal{D}} (2\pi\lambda)^K r_1\cdots r_K e^{-\pi\lambda r_K^2} \int_{-\infty}^{\infty} e^{-2\pi j\gamma_{th}s\sigma^2} \times \frac{\mathcal{L}_P(-2\pi js)-1}{2\pi js} \mathrm{d}s\mathrm{d}r, \quad (12)$$

where $\mathcal{L}_P(s)$ *is given in (11).*

Proof: Since SINR $\approx$ SNR, $I_L = I_N = 0$. Then, according to (32), Corollary 2 can be readily obtained. □

Theorem 3: The conditional ergodic capacity with Nakagami fading is

$$C_{cond} = \frac{1}{\ln 2} \int_0^{\infty} \frac{e^{-s\sigma^2}}{s} e^{-(Q_L(s)+Q_N(s))} (1-\mathcal{L}_P(s)) \mathrm{d}s, \quad (13)$$

where $Q_L(s)$, $Q_N(s)$ *and* $\mathcal{L}_P(s)$ *are given in (9), (10) and (11), respectively. By substituting (7) and (13) into (6), the downlink ergodic capacity with Nakagami fading is given by*

$$C = \frac{1}{\ln 2} \int\cdots\int_{\mathcal{D}} (2\pi\lambda)^K r_1\cdots r_K e^{-\pi\lambda r_K^2} \times \int_0^{\infty} \frac{e^{-s\sigma^2}}{s} e^{-(Q_L(s)+Q_N(s))} (1-\mathcal{L}_P(s)) \mathrm{d}s\mathrm{d}r. \quad (14)$$

Proof: The proof is given in Appendix B. □

Corollary 4: The approximate ergodic capacity in noise-limited scenarios with Nakagami fading can be written as

$$\widetilde{C} = \frac{1}{\ln 2} \int\cdots\int_{\mathcal{D}} (2\pi\lambda)^K r_1\cdots r_K e^{-\pi\lambda r_K^2} \times \int_0^{\infty} \frac{e^{-s\sigma^2}}{s} (1-\mathcal{L}_P(s)) \mathrm{d}s\mathrm{d}r, \quad (15)$$

where $\mathcal{L}_P(s)$ *is given in (11).*

Proof: Corollary 4 can be easily obtained from the proof of Theorem 3 and $I_L = I_N = 0$. □

C. COVERAGE PROBABILITY AND ERGODIC CAPACITY WITH RAYLEIGH FADING

In this subsection, we analyze the coverage probability and ergodic capacity when the small-scale fading is Rayleigh fading, i.e., $|\xi_l|^2 \sim \exp(\mu)$.[6] The coverage probability and ergodic capacity for user-centric dense network with Rayleigh fading are given in Theorem 5 and 7, respectively. Moreover, by assuming that SINR $\approx$ SNR, we present the approximate coverage probability and ergodic capacity with Rayleigh fading in Corollary 6 and 8.

Theorem 5: The expression for coverage probability with Rayleigh fading is given by

$$\Pr = \int\cdots\int_{\mathcal{D}} (2\pi\lambda)^K r_1\cdots r_K e^{-\pi\lambda r_K^2} \int_{-\infty}^{\infty} e^{-2\pi j\gamma_{th}s\sigma^2} \times e^{-V_L(2\pi j\gamma_{th}s)} e^{-V_N(2\pi j\gamma_{th}s)} \frac{\mathcal{L}_P(-2\pi js)-1}{2\pi js} \mathrm{d}s\mathrm{d}r, \quad (16)$$

where

$$V_L(s) = \sum_{n=1}^{2} 2\pi\lambda b_n \int_{r_K}^{\infty} H(\mu sa_nC_Lx^{-\alpha_L}) p(x) x \mathrm{d}x, \quad (17)$$

$$V_N(s) = \sum_{n=1}^{2} 2\pi\lambda b_n \int_{r_K}^{\infty} H(\mu sa_nC_Nx^{-\alpha_N})(1-p(x)) x \mathrm{d}x, \quad (18)$$

[6]Note that when $\mu = 1$ and $N_L = 1$ (or $N_N = 1$), Rayleigh fading is equivalent to Nakagami fading.

$$\mathcal{L}_P(s) = \prod_{k=1}^{K}(1 - H(\mu s M C_L r_k^{-\alpha_L})), \quad (19)$$

$H(x) = 1 - 1/(1+x)$, a_n and b_n are defined in Subsection II-B.

Proof: The proof is given in Appendix C. □

Corollary 6: Obviously, the approximate coverage probability in noise-limited scenarios with Rayleigh fading can be written as

$$\widetilde{\Pr} = \int \cdots \int_{\mathcal{D}} (2\pi\lambda)^K r_1 \cdots r_K e^{-\pi\lambda r_K^2} \times \int_{-\infty}^{\infty} e^{-2\pi j \gamma_{th} s\sigma^2} \frac{\mathcal{L}_P(-2\pi j s) - 1}{2\pi j s} \mathrm{d}s\mathrm{d}r, \quad (20)$$

where $\mathcal{L}_P(s)$ is given in (19).

Theorem 7: The conditional ergodic capacity with Rayleigh fading is

$$C_{cond} = \frac{1}{\ln 2} \int_0^{\infty} \frac{e^{-s\sigma^2}}{s} e^{-(V_L(s)+V_N(s))} (1 - \mathcal{L}_P(s)) \, \mathrm{d}s, \quad (21)$$

where $V_L(s)$, $V_N(s)$ and $\mathcal{L}_P(s)$ are given in (17), (18) and (19), respectively. By substituting (7) and (21) into (6), the downlink ergodic capacity with Rayleigh fading can be given by

$$C = \frac{1}{\ln 2} \int \cdots \int_{\mathcal{D}} (2\pi\lambda)^K r_1 \cdots r_K e^{-\pi\lambda r_K^2} \times \int_0^{\infty} \frac{e^{-s\sigma^2}}{s} e^{-(V_L(s)+V_N(s))} (1 - \mathcal{L}_P(s)) \, \mathrm{d}s\mathrm{d}r. \quad (22)$$

Proof: The detailed procedure is similar to that in Appendix B. □

Corollary 8: Apparently, the approximate ergodic capacity in noise-limited scenarios with Rayleigh fading can be written as

$$\widetilde{C} = \frac{1}{\ln 2} \int \cdots \int_{\mathcal{D}} (2\pi\lambda)^K r_1 \cdots r_K e^{-\pi\lambda r_K^2} \times \int_0^{\infty} \frac{e^{-s\sigma^2}}{s} (1 - \mathcal{L}_P(s)) \, \mathrm{d}s\mathrm{d}r, \quad (23)$$

where $\mathcal{L}_P(s)$ is given in (19).

D. COVERAGE PROBABILITY AND ERGODIC CAPACITY WITHOUT SMALL-SCALE FADING

In this subsection, we study the coverage probability and ergodic capacity without the small-scale fading, i.e., $|\xi_k|^2 = 1$. The SINR is rewritten as

$$\gamma' = \frac{\sum_{k \in \Phi \cap \mathcal{B}(0,r_K)} M C_L r_k^{-\alpha_L}}{I_L' + I_N' + \sigma^2}, \quad (24)$$

where $I_L' = \sum_{l \in \Phi_L \cap \bar{\mathcal{B}}(0,r_K)} G_l C_L r_l^{-\alpha_L}$ and $I_N' = \sum_{l \in \Phi_N \cap \bar{\mathcal{B}}(0,r_K)} G_l C_N r_l^{-\alpha_N}$. Then, the coverage probability and ergodic capacity for user-centric dense network with no fading are given in Theorem 9 and 11. The approximate expressions for coverage probability and ergodic capacity without fading distribution are given in Corollary 10 and 12, respectively.

Theorem 9: The coverage probability without small-scale fading is given by

$$\Pr = \int \cdots \int_{\mathcal{D}} (2\pi\lambda)^K r_1 \cdots r_K e^{-\pi\lambda r_K^2} \int_{-\infty}^{\infty} e^{-2\pi j \gamma_{th} s\sigma^2} \times e^{-W_L(2\pi j\gamma_{th}s)} e^{-W_N(2\pi j\gamma_{th}s)} \times \frac{e^{-2\pi j s \sum_{k=1}^{K} M C_L r_k^{-\alpha_L}} - 1}{2\pi j s} \mathrm{d}s\mathrm{d}r, \quad (25)$$

where

$$W_L(s) = 2\pi\lambda \sum_{n=1}^{2} b_n \int_{r_K}^{\infty} \left(1 - e^{-s a_n C_L x^{-\alpha_L}}\right) p(x) x \mathrm{d}x, \quad (26)$$

$$W_N(s) = 2\pi\lambda \sum_{n=1}^{2} b_n \int_{r_K}^{\infty} \left(1 - e^{-s a_n C_N x^{-\alpha_N}}\right) (1 - p(x)) x \mathrm{d}x, \quad (27)$$

a_n and b_n are defined in Subsection II-B.

Proof: The proof is given in Appendix D. □

Corollary 10: Obviously, the approximate coverage probability in noise-limited scenarios without fading can be written as

$$\widetilde{\Pr} = \int \cdots \int_{\mathcal{D}} (2\pi\lambda)^K r_1 \cdots r_K e^{-\pi\lambda r_K^2} \int_{-\infty}^{\infty} e^{-2\pi j \gamma_{th} s\sigma^2} \times \frac{e^{-2\pi j s \sum_{k=1}^{K} M C_L r_k^{-\alpha_L}} - 1}{2\pi j s} \mathrm{d}s\mathrm{d}r. \quad (28)$$

Theorem 11: The conditional ergodic capacity without fading is

$$C_{cond} = \frac{1}{\ln 2} \int_0^{\infty} \frac{e^{-s\sigma^2}}{s} e^{-(W_L(s)+W_N(s))} \times \left(1 - \prod_{k=1}^{K} e^{-s M C_L r_k^{-\alpha_L}}\right) \mathrm{d}s, \quad (29)$$

where $W_L(s)$ and $W_N(s)$ are given in (26) and (27), respectively. By substituting (7) and (29) into (6), the downlink ergodic capacity with no fading is given by

$$C = \frac{1}{\ln 2} \int \cdots \int_{\mathcal{D}} (2\pi\lambda)^K r_1 \cdots r_K e^{-\pi\lambda r_K^2} \int_0^{\infty} \frac{e^{-s\sigma^2}}{s} \times e^{-(W_L(x)+W_N(x))} \left(1 - \prod_{k=1}^{K} e^{-s M C_L r_k^{-\alpha_L}}\right) \mathrm{d}s\mathrm{d}r. \quad (30)$$

Proof: The detailed procedure is similar to that in Appendix B. □

Corollary 12: Obviously, the approximate ergodic capacity in noise-limited scenarios without fading can be written as

$$\widetilde{C} = \frac{1}{\ln 2} \int \cdots \int_{\mathcal{D}} (2\pi\lambda)^K r_1 \cdots r_K e^{-\pi\lambda r_K^2} \int_0^{\infty} \frac{e^{-s\sigma^2}}{s} \times \left(1 - \prod_{k=1}^{K} e^{-s M C_L r_k^{-\alpha_L}}\right) \mathrm{d}s\mathrm{d}r. \quad (31)$$

IV. NUMERICAL RESULTS

In this section, we provide some numerical results to validate our analysis. We consider the APs are distributed in a circular region with radius $R = 100\ m$ and the UE is located at the origin. The mmWave is assumed to be operated at 73 GHz and the bandwidth is $B = 2$ GHz. The transmitting power of mmWave AP is $P_t = 30$ dBm. The normalized noise power is $\sigma^2 = -174$ dBm/Hz$+10\log_{10}(B)+$noise figure of 10dB$-P_t$. The main lobe gain is $M = 18$ dB, side lobe gain is $m = -2$ dB, and beam-width is $\theta_b = 10^o$ [21]. The parameter of the Rayleigh fading is $\mu = 1$ [22]. Unless stated otherwise, the parameters are given as follows. The density[7] $\lambda = 2e^{-3}$. The parameter in LOS probability function is $\beta = 0.0071$. $\alpha_L = 2$, $\alpha_N = 4$, $C_L = C_N = 10^{-7}$, $N_L = 3$ and $N_N = 2$ [19]. The simulation results are obtained by averaging over 1000 channel realizations. The Riemann sums [30] are used to compute these complicated expressions approximatively.

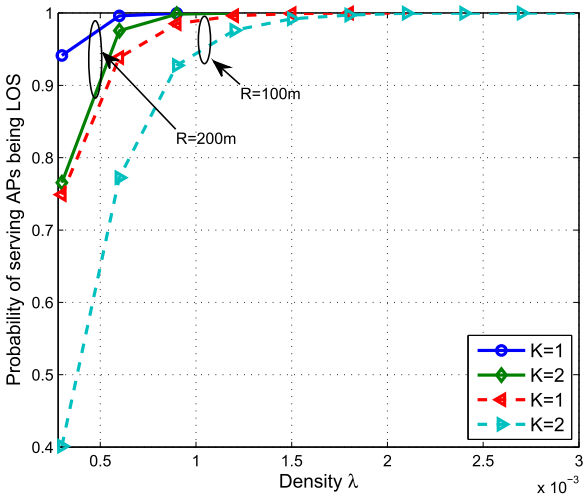

FIGURE 3. The probability of the serving APs being in LOS with different density λ and zone radius R.

Recall that the serving APs for the UE are assumed to be in LOS with dense deployment. To justify this assumption, we present the probability of the serving APs being in LOS versus the AP density in Fig. 3. From this figure, we can find that the probability increases with density and tends to be 1, which verifies our assumption. In addition, the probability increases with the increase of R and decrease of K. The reason is that the average number of APs N increases greatly with R, due to $N = \lambda\pi R^2$. Therefore, the distances between the serving APs to the UE are reduced, which increase the probability.

In the following, we provide extensive results to study the impact of key factors on the coverage probability and ergodic capacity. Note that, the results in all figures are obtained based on the computation of analytical expressions unless otherwise stated.

[7] According to the definition of homogeneous PPP, the average number of APs $N = \lambda\pi R^2 \approx 62$, which means that the networks are ultra-dense in the simulation environments.

A. COVERAGE PROBABILITY

Fig. 4 presents the coverage probability with AP cooperation (i.e., $K = 2$) under three small-scale fading distributions. It can be seen that the analytical results for coverage probability in (8), (16) and (25) match well with[8] the corresponding simulation results. As expected, the coverage probabilities among three different fading distributions decrease with the targeted SINR threshold. Moreover, we find that when $\gamma_{th} \leqslant 5\ dB$, the coverage probabilities decrease slightly, while significantly when $\gamma_{th} > 5\ dB$. It is mainly because we assume that the K-closest APs are chosen to serve the UE and they are all in LOS, which contribute to a high desired signal power.

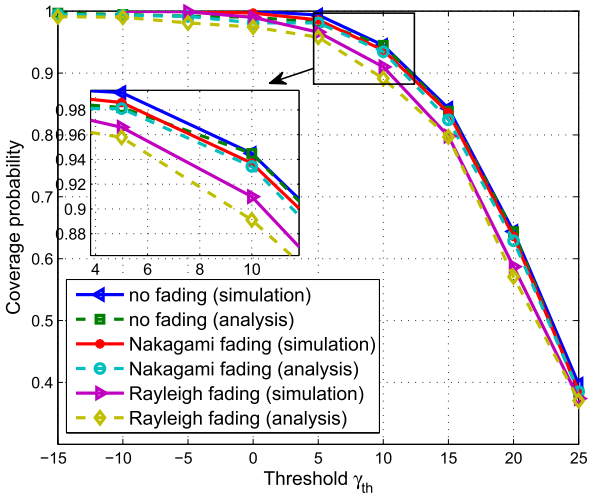

FIGURE 4. Coverage probability with different threshold, where $K = 2$.

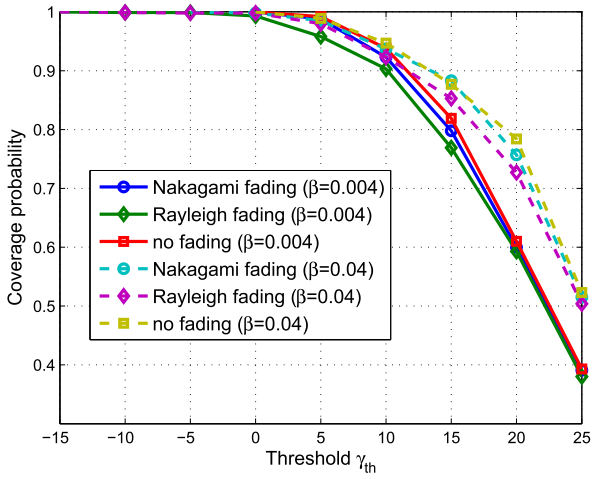

FIGURE 5. Coverage probability with different threshold under three small-scale fading distributions and two blockage parameters, where $K = 2$.

Fig. 5 shows the impacts of blockage parameter on the coverage probability. It can be easily seen that the coverage probabilities among three different fading distributions increase

[8] Actually, the analytical results are marginally smaller than the simulation results, which arises from the approximate calculation methods.

with the blockage parameter β, which is consistent with [22]. The reason can be explained as follows. According to the LOS probability function $e^{-\beta r}$, a larger β will yield a smaller number of LOS interfering APs. Thus, the interference power decreases with β, which results in the increase of SINR and coverage probability. On the other hand, the coverage probability without small-scale fading is the greatest among the three fading distributions.

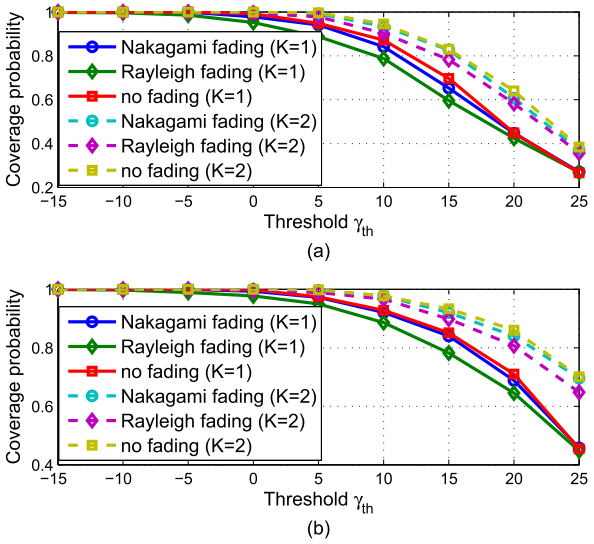

FIGURE 6. Coverage probability versus threshold with two cooperation APs ($K = 2$) and without AP cooperation ($K = 1$) under different simulation parameters. In (a), $\alpha_L = 2$, $\alpha_N = 4$. In (b), $\alpha_L = 3$, $\alpha_N = 5$.

Fig. 6 shows the comparison of coverage probability between AP cooperation (i.e., $K = 2$) and non-cooperation (i.e., $K = 1$) under different simulation setups. As expected, the coverage probability with AP cooperation is greater than that without AP cooperation in both Fig. 6 (a) and (b). The reason is apparent and can be explained as follows. With given AP density λ, the desired signal power increases with the number of serving APs K, which leads to the increase in SINR. In addition, the coverage performance in (b) is better than that in (a) due to the lower path loss.

A comparison of the coverage probability between with and without applying the noise-limited approximation under different density is shown in Fig. 7. This figure reveals the fact that the coverage probability when assuming that SINR $\approx$ SNR is greater than that without this assumption. In addition, it can be seen that the approximation performance when $K = 2$ is better than that when $K = 1$. To make it clear, we calculate the average approximation performance, defined as the average difference value of coverage probability between the noise-limited approximation and no approximation, given in Table 1. The reason can be explained as follows. When K increases, the number of interfering APs decreases, which results in the decrease of interference power. Thus, the thermal noise power dominates the interference power. In other words, the difference between SNR and SINR becomes smaller. Additionally, the approximation

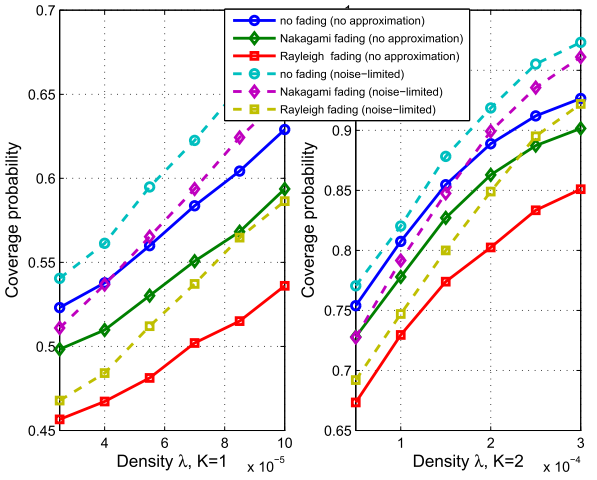

FIGURE 7. Comparison between coverage probability with and without noise-limited approximation, where $\gamma_{th} = 20$ *dB* and $\beta = 0.04$.

TABLE 1. Average difference values of coverage probability.

K \ Fading	Nakagami	Rayleigh	No fading
1	0.0706	0.0656	0.0635
2	0.0356	0.0518	0.0336

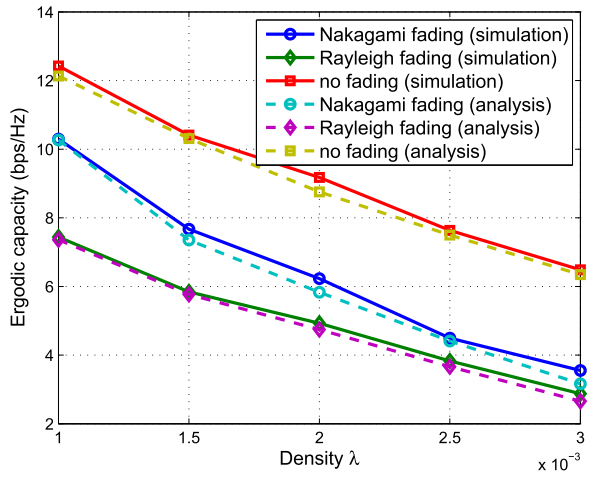

FIGURE 8. Ergodic capacity with different density under three small-scale fading distributions, where $K = 2$.

performance decrease with the increase of density λ. This is because that the number of interfering APs increase with λ, resulting in the increment of interference power. As a consequence, the interference power cannot be ignored compared with the noise power.

B. ERGODIC CAPACITY

Fig. 8 shows the ergodic capacity with AP cooperation (i.e., $K = 2$) under three small-scale fading distributions. Firstly, the analytical ergodic capacity expressions in (14), (22) and (30) match well with the simulation results. Secondly, as expected, the ergodic capacity is always the highest when no small-scale fading is assumed. It is also interesting to find that the ergodic capacity under Nakagami

fading is higher than that under Rayleigh fading. Thirdly, the ergodic capacity decreases with the AP density λ, regardless of the fading model. The reason is that, when the density increases, the number of interfering APs increases, while the number of serving APs remains unchanged. Thus, the ergodic capacity is degraded.

Fig. 9 shows the impacts of blockage, path loss and antenna parameters on the ergodic capacity. It can be seen from both (a) and (b) that the ergodic capacity increases with the blockage parameter β under all three fading distributions, which is consistent with [22]. This is because that the blockage probability of the LOS interfering links increases with β, and so does the number of NLOS APs. As a result, the total interference power decreases and the ergodic capacity increases. Additionally, the ergodic capacity in (b) is greater than that in (a) since higher antenna gain and lower NLOS path loss.

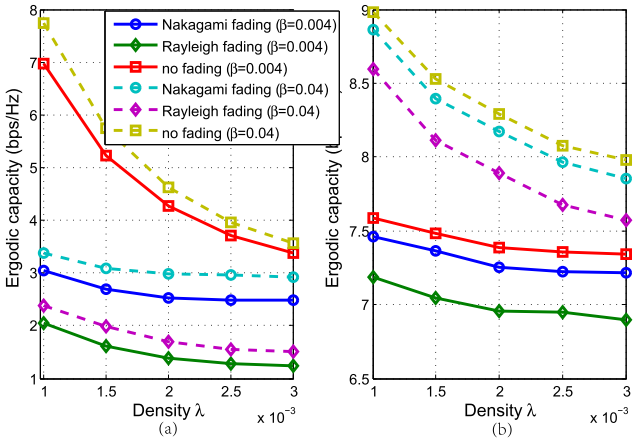

FIGURE 9. Ergodic capacity versus density under three small-scale fading distributions and two blockage parameters, where $K = 1$. In (a), $\alpha_L = 2$, $\alpha_N = 4$, $M = 18$ dB, and $m = -2$ dB. In (b), $\alpha_L = 2$, $\alpha_N = 5$, $M = 20$ dB, and $m = -4$ dB.

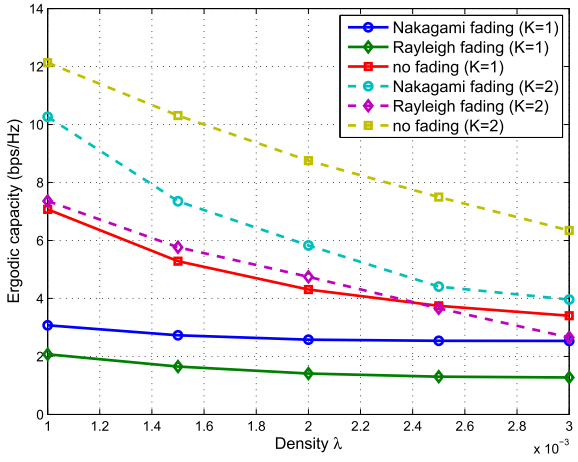

FIGURE 10. Ergodic capacity with two cooperation APs ($K = 2$) and without AP cooperation ($K = 1$).

Fig. 10 compares the ergodic capacity achieved under AP cooperation with that achieved under non-cooperation. As expected, the AP cooperation scheme achieves higher ergodic capacity than the non-cooperation scheme. In addition, AP cooperation provides higher capacity gain when the AP density is low. The reasons can be explained as follows. At low AP densities, the desired signal power, and hence the SINR, increase with the number of cooperative APs K, which improves the capacity performance. On the other hand, when the AP density becomes large enough (e.g., greater than 0.0025), the interference power dominates the desired power, offsetting the cooperative gain.

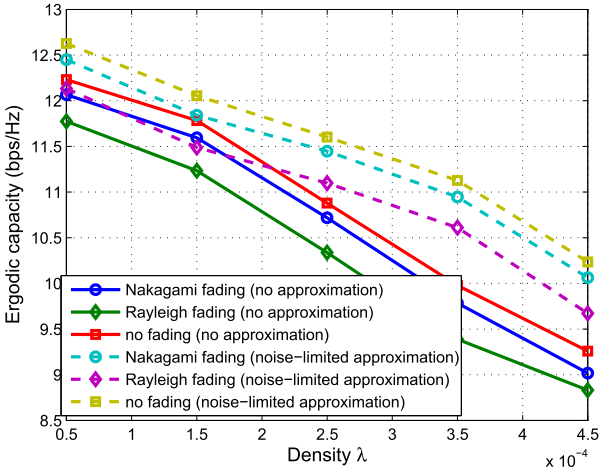

FIGURE 11. Ergodic capacity with and without noise-limited approximation, where $K = 2$ and $\beta = 0.4$.

In Fig. 11, we present the ergodic capacity and its approximate results obtained by the noise-limited approximation. It can be seen that the approximation performance of ergodic capacity under three fading distributions decrease with the AP density. This phenomenon is due to the fact that the interference power dominates when the density is large, which is consistent with the conclusion in [31]. In the other words, mmWave systems with specific scenarios (e.g., low density and high blockage parameter) tend to be noise-limited.

V. CONCLUSION

This paper analyzed the coverage probability and ergodic capacity of the mmWave user-centric dense networks where multiple APs and blockages are randomly distributed. Taking into account the AP location randomness, directional beamforming, blockage-dependent path loss and the AP cooperation, we derived the expressions for coverage probability and ergodic capacity under three different small-scale fading distributions (i.e., Nakagami, Rayleigh and no fading). To make it tractable, we propose a strong but reasonable assumption (i.e., the serving APs are assumed to be in LOS with dense deployment), which was verified by the simulation results. By applying the noise-limited approximation (i.e, SINR $\approx$ SNR), we presented the approximate expressions for coverage probability and ergodic capacity. Numerical results validated our analytical expressions and showed that the AP cooperation can provide high coverage performance and distinct capacity gain in a lower AP density region. In addition,

the noise-limited characteristic of mmWave communications is closely related to the AP density.

APPENDIX A
PROOF OF THEOREM 1

The coverage probability with Nakagami fading distribution is given by

$$\begin{aligned}\Pr &= \mathbb{P}\left(\frac{P}{I_L+I_N+\sigma^2} > \gamma_{th}\right)\\ &= \mathbb{E}_{\mathbf{r}}\left[\mathbb{P}\left(P > \gamma_{th}(I_L+I_N+\sigma^2)|\mathbf{r}\right)\right]\\ &\overset{(a)}{=} \int\cdots\int_{\mathcal{D}} f_{r_1,\cdots,r_K}(r_1,\cdots,r_K)\int_{-\infty}^{\infty} e^{-2\pi j\gamma_{th}s\sigma^2}\\ &\quad\times\mathcal{L}_{I_L}(2\pi j\gamma_{th}s)\mathcal{L}_{I_N}(2\pi j\gamma_{th}s)\frac{\mathcal{L}_P(-2\pi js)-1}{2\pi js}\mathrm{d}s\mathrm{d}\boldsymbol{r},\end{aligned} \tag{32}$$

where $P=\sum_{k\in\Phi\cap\mathcal{B}(0,r_K)} MC_L r_k^{-\alpha_L}|\xi_k|^2$, (a) follows from [29, Proposition 2.2], $\mathcal{L}_X(s)$ is the Laplace Transformation (LT) of X, and $f_{r_1,\cdots,r_K}(r_1,\cdots,r_K)$ is given in (7).

Now, we need to compute the LT of I_L, I_N and P. The LT of I_L is derived as follows.

$$\begin{aligned}\mathcal{L}_{I_L}(s) &= \mathbb{E}_{\Phi_L,\mathbf{G},\boldsymbol{\xi}}\left[e^{-s\sum_{l\in\Phi_L\cap\bar{\mathcal{B}}(0,r_K)} G_l C_L r_l^{-\alpha_L}|\xi_l|^2}\right]\\ &\overset{(a)}{=} e^{-2\pi\lambda\sum_{n=1}^{2} b_n\int_{r_K}^{\infty}\left(1-\mathbb{E}_{\xi}\left[e^{-sa_nC_Lx^{-\alpha_L}|\xi|^2}\right]\right)p(x)x\mathrm{d}x}\\ &\overset{(b)}{=} \prod_{n=1}^{2} e^{-2\pi\lambda b_n\int_{r_K}^{\infty}\left(1-1/(1+sa_nC_Lx^{-\alpha_L}/N_L)^{N_L}\right)p(x)x\mathrm{d}x}\\ &= e^{-Q_L(s)},\end{aligned} \tag{33}$$

where $p(x)$ is the LOS probability function, a_n and b_n are given in Subsection II-B for $n\in\{1,2\}$. (a) follows from the Laplace function of the PPP Φ_L [32]. (b) is obtained by calculating the moment generating function (MGF) of $|\xi|^2$, where $|\xi|^2$ obeys the normalized Gamma distribution with parameter N_L (i.e., $|\xi_k|^2\sim\Gamma(N_L,1/N_L)$).

In a similar way, the small-scale fading coefficient $|\xi_l|^2$ of the NLOS interfering link is a normalized Gamma r.v. with N_N. Thus, the LT of I_N is given by

$$\begin{aligned}\mathcal{L}_{I_N}(s) &= \mathbb{E}_{\Phi_N,\mathbf{G},\boldsymbol{\xi}}\left[e^{-s\sum_{l\in\Phi_N\cap\bar{\mathcal{B}}(0,r_K)} G_l C_N r_l^{-\alpha_N}|\xi_l|^2}\right]\\ &= e^{-2\pi\lambda\sum_{n=1}^{2} b_n\int_{r_K}^{\infty}\left(1-\mathbb{E}_{\xi}\left[e^{-sa_nC_Nx^{-\alpha_N}|\xi|^2}\right]\right)(1-p(x))x\mathrm{d}x}\\ &= \prod_{n=1}^{2} e^{-2\pi\lambda b_n\int_{r_K}^{\infty}\left(1-1/(1+sa_nC_Nx^{-\alpha_N}/N_N)^{N_N}\right)(1-p(x))x\mathrm{d}x}\\ &= e^{-Q_N(s)}.\end{aligned} \tag{34}$$

Before deriving the LT of P in (32), we first let $p_k = MC_L r_k^{-\alpha_L}|\xi_k|^2$, $k=1,\cdots,K$. The LT of p_k can be given by

$$\begin{aligned}\mathcal{L}_{p_k}(s) &= \mathbb{E}_{\xi_k}[e^{-sp_k}] = \mathbb{E}_{\xi_k}\left[e^{-sMC_Lr_k^{-\alpha_L}|\xi_k|^2}\right]\\ &\overset{(a)}{=} \frac{1}{(1+sMC_Lr_k^{-\alpha_L}/N_L)^{N_L}},\end{aligned}$$

where $|\xi_k|^2\sim\Gamma(N_L,1/N_L)$ and (a) is obtained by computing its MGF. Because of the independence among $p_1,\cdots,p_K$, the PDF of $P=\sum_{k=1}^{K}p_k$ can be given by

$$f_P(z) = f_{p_1}(z)*\cdots*f_{p_K}(z),$$

where $*$ is convolution operation and $f_{p_k}(z)$ is the PDF of p_k. Then, the LT of P can be obtained as

$$\mathcal{L}_P(s)=\prod_{k=1}^{K}\mathcal{L}_{p_k}(s)=\prod_{k=1}^{K}\frac{1}{(1+sMC_Lr_k^{-\alpha_L}/N_L)^{N_L}}. \tag{35}$$

Thus, (8) is obtained by substituting (33), (34) and (35) into (32).

APPENDIX B
PROOF OF THEOREM 3

Conditioning on the serving APs being at distances $r_1\leqslant\cdots\leqslant r_K$ from the typical UE and the interfering APs being outside the distance r_K, the conditional ergodic capacity is given by

$$\begin{aligned}C_{\text{cond}} &= \mathbb{E}_{\mathbf{G},\boldsymbol{\xi}}\left[\log_2\left(1+\frac{\sum_{k\in\Phi\cap\mathcal{B}(0,r_K)} MC_Lr_k^{-\alpha_L}|\xi_k|^2}{I_L+I_N+\sigma^2}\right)\right]\\ &\overset{(a)}{=} \frac{1}{\ln 2}\mathbb{E}\left[\int_0^{\infty}\frac{e^{-s\sigma^2}}{s}e^{-s(I_L+I_N)}(1-e^{-sP})\right]\mathrm{d}s\\ &\overset{(b)}{=} \frac{1}{\ln 2}\int_0^{\infty}\mathbb{E}\left[\frac{e^{-s\sigma^2}}{s}e^{-sI_L}e^{-sI_N}(1-e^{-sP})\right]\mathrm{d}s\\ &\overset{(c)}{=} \frac{1}{\ln 2}\int_0^{\infty}\frac{e^{-s\sigma^2}}{s}\mathcal{L}_{I_L}(s)\mathcal{L}_{I_N}(s)(1-\mathcal{L}_P(s))\mathrm{d}s,\end{aligned} \tag{36}$$

where (a) follows from [33, Lemma 1]

$$\ln(1+x)=\int_0^{\infty}\frac{1}{z}(1-e^{-xz})e^{-z}\mathrm{d}z,$$

and replaces z with $s(I_L+I_N+\sigma^2)$. Step (b) is obtained by changing the order of integration and expectation operation and (c) is due to the fact that I_L, I_N and P are independent. $\mathcal{L}_{I_L}(s)$, $\mathcal{L}_{I_N}(s)$ and $\mathcal{L}_P(s)$ are given in (33), (34) and (35), respectively.

Thus, (13) is obtained by substituting (33), (34) and (35) into (36).

APPENDIX C
PROOF OF THEOREM 5

With a similar procedure in (32), the coverage probability with Rayleigh fading distribution is given by

$$\begin{aligned}\Pr = &\int\cdots\int_{\mathcal{D}} f_{r_1,\cdots,r_K}(r_1,\cdots,r_K)\int_{-\infty}^{\infty} e^{-2\pi j\gamma_{th}s\sigma^2}\\ &\times\mathcal{L}_{I_L}(2\pi j\gamma_{th}s)\mathcal{L}_{I_N}(2\pi j\gamma_{th}s)\frac{\mathcal{L}_P(-2\pi js)-1}{2\pi js}\mathrm{d}s\mathrm{d}\boldsymbol{r}.\end{aligned} \tag{37}$$

In the following, we only need to compute the LT of P, I_L and I_N with Rayleigh fading.

Let $g_k = |\xi_k|^2$ and then $p_k = MC_L r_k^{-\alpha_L} g_k, k = 1, \cdots, K$.

$$\mathcal{L}_{p_k}(s) = \mathbb{E}_{g_k}\left[e^{-sMC_L r_k^{-\alpha_L} g_k}\right] \overset{(a)}{=} \frac{1}{1+\mu s MC_L r_k^{-\alpha_L}},$$

where (a) follows from the fact that $g_k \sim \exp(\mu)$ and computing its MGF. Then, similar to (35), the LT of P with Rayleigh fading is given by

$$\mathcal{L}_P(s) = \prod_{k=1}^{K} \mathcal{L}_{p_k}(s) = \prod_{k=1}^{K} \frac{1}{1+\mu s MC_L r_k^{-\alpha_L}}. \tag{38}$$

The LT of I_L with Rayleigh fading can be derived as

$$\begin{aligned}\mathcal{L}_{I_L}(s) &= \mathbb{E}_{\Phi_L,\mathbf{G},\boldsymbol{\xi}}\left[e^{-s\sum_{l\in\Phi_L\cap\bar{\mathcal{B}}(0,r_K)} G_l C_L r_l^{-\alpha_L}|\xi_l|^2}\right] \\ &\overset{(a)}{=} e^{-2\pi\lambda\sum_{n=1}^{2} b_n \int_{r_K}^{\infty}\left(1-\mathbb{E}_g\left[e^{-sa_nC_L x^{-\alpha_L}}\right]\right)p(x)x\mathrm{d}x} \\ &\overset{(b)}{=} \prod_{n=1}^{2} e^{-2\pi\lambda b_n \int_{r_K}^{\infty}(1-1/(1+\mu s a_n C_L x^{-\alpha_L}))p(x)x\mathrm{d}x} \\ &= e^{-V_L(s)}, \end{aligned} \tag{39}$$

where for $n \in \{1, 2\}$, a_n and b_n are defined in Subsection II-B; (a) is obtained by computing the Laplace function of the PPP Φ_L [32]; (b) is obtained by computing the MGF of g.

Similarly, the LT of I_N with Rayleigh fading is given by

$$\begin{aligned}\mathcal{L}_{I_N}(s) &= \prod_{n=1}^{2} e^{-2\pi\lambda b_n \int_{r_K}^{\infty}(1-1/(1+\mu s a_n C_N x^{-\alpha_N}))(1-p(x))x\mathrm{d}x} \\ &= e^{-V_N(s)}. \end{aligned} \tag{40}$$

Thus, (16) can be obtained by substituting (38), (39) and (40) into (37).

APPENDIX D
PROOF OF THEOREM 9

With a similar procedure in (32), the coverage probability with no fading distribution is given by

$$\begin{aligned}\Pr &= \mathbb{P}\left(\frac{\sum_{k=1}^{K} MC_L r_k^{-\alpha_L}}{I'_L + I'_N + \sigma^2} > \gamma_{th}\right) \\ &= \int\cdots\int_{\mathcal{D}} f_{r_1,\cdots,r_K}(r_1,\cdots,r_K)\int_{-\infty}^{\infty} e^{-2\pi j\gamma_{th}s\sigma^2} \\ &\quad\times \mathcal{L}_{I'_L}(2\pi j\gamma_{th}s)\mathcal{L}_{I'_N}(2\pi j\gamma_{th}s) \\ &\quad\times \frac{e^{-2\pi j s\sum_{k=1}^{K} MC_L r_k^{-\alpha_L}} - 1}{2\pi j s}\mathrm{d}s\mathrm{d}\boldsymbol{r}. \end{aligned} \tag{41}$$

The detailed derivations of $\mathcal{L}_{I'_L}(s)$ and $\mathcal{L}_{I'_N}(s)$ are similar to (33) and (34), respectively. Thus, we only present the final results as follows.

$$\begin{aligned}\mathcal{L}_{I'_L}(s) &= e^{-2\pi\lambda\sum_{n=1}^{2} b_n \int_{r_K}^{\infty}\left(1-e^{-sa_nC_L x^{-\alpha_L}}\right)p(x)x\mathrm{d}x} \\ &= e^{-W_L(s)}, \end{aligned} \tag{42}$$

$$\begin{aligned}\mathcal{L}_{I'_N}(s) &= e^{-2\pi\lambda\sum_{n=1}^{2} b_n \int_{r_K}^{\infty}\left(1-e^{-sa_nC_N x^{-\alpha_N}}\right)(1-p(x))x\mathrm{d}x} \\ &= e^{-W_N(s)}. \end{aligned} \tag{43}$$

Then, (25) is obtained by substituting (42) and (43) into (41).

REFERENCES

[1] C. V. N. I. Cisco, "Global mobile data traffic forecast update, 2016–2021," White Paper, Feb. 2017.

[2] F. Boccardi, R. W. Heath, A. Lozano, T. L. Marzetta, and P. Popovski, "Five disruptive technology directions for 5G," *IEEE Commun. Mag.*, vol. 52, no. 2, pp. 74–80, Feb. 2014.

[3] Y. Zhang and Y. J. Zhang, "User-centric virtual cell design for cloud radio access networks," in *Proc. IEEE Int. Workshop Signal Process. Adv. Wireless Commun. (SPAWC)*, Jun. 2014, pp. 249–253.

[4] L. Dai, "An uplink capacity analysis of the distributed antenna system (DAS): From cellular DAS to DAS with virtual cells," *IEEE Trans. Wireless Commun.*, vol. 13, no. 5, pp. 2717–2731, May 2014.

[5] A. Abdelreheem, E. M. Mohamed, and H. Esmaiel, "Location-based millimeter wave multi-level beamforming using compressive sensing," *IEEE Commun. Lett.*, vol. 22, no. 1, pp. 185–188, Jan. 2018.

[6] S. F. Yunas, M. Valkama, and J. Niemelä, "Spectral and energy efficiency of ultra-dense networks under different deployment strategies," *IEEE Commun. Mag.*, vol. 53, no. 1, pp. 90–100, Jan. 2015.

[7] R. Baldemair *et al.*, "Ultra-dense networks in millimeter-wave frequencies," *IEEE Commun. Mag.*, vol. 53, no. 1, pp. 202–208, Jan. 2015.

[8] X. Yu, J. Zhang, and K. B. Letaief, "Coverage analysis for dense millimeter wave cellular networks: The impact of array size," in *Proc. IEEE Wireless Commun. Netw. Conf. (WCNC)*, Apr. 2016, pp. 1–6.

[9] T. E. Bogale and L. B. Le, "Massive MIMO and mmWave for 5G wireless HetNet: Potential benefits and challenges," *IEEE Veh. Technol. Mag.*, vol. 11, no. 1, pp. 64–75, Mar. 2016.

[10] M. N. Kulkarni, S. Singh, and J. G. Andrews, "Coverage and rate trends in dense urban mmWave cellular networks," in *Proc. IEEE Global Commun. Conf. (GLOBECOM)*, Dec. 2014, pp. 3809–3814.

[11] V. Petrov *et al.*, "Dynamic multi-connectivity performance in ultra-dense urban mmWave deployments," *IEEE J. Sel. Areas Commun.*, vol. 35, no. 9, pp. 2038–2055, Sep. 2017.

[12] S. Jia, L. Liu, H. Jiang, Z. Zhao, M. Peng, and Y. Li, "Performance analysis of multicasting in cloud-radio access networks," in *Proc. IEEE Veh. Technol. Conf. (VTC)*, May 2016, pp. 1–5.

[13] Z. Zhao, M. Peng, Z. Ding, C. Wang, and H. V. Poor, "Cluster formation in cloud-radio access networks: Performance analysis and algorithms design," in *Proc. IEEE Int. Conf. Commun. (ICC)*, Jun. 2015, pp. 3903–3908.

[14] Z. Yang, Z. Ding, and P. Fan, "Performance analysis of cloud radio access networks with uniformly distributed base stations," *IEEE Trans. Veh. Technol.*, vol. 65, no. 1, pp. 472–477, Jan. 2016.

[15] F. A. Khan, H. He, J. Xue, and T. Ratnarajah, "Performance analysis of cloud radio access networks with distributed multiple antenna remote radio heads," *IEEE Trans. Signal Process.*, vol. 63, no. 18, pp. 4784–4799, Sep. 2015.

[16] M. Peng, S. Yan, and H. V. Poor, "Ergodic capacity analysis of remote radio head associations in cloud radio access networks," *IEEE Wireless Commun. Lett.*, vol. 3, no. 4, pp. 365–368, Aug. 2014.

[17] J. G. Andrews, T. Bai, M. N. Kulkarni, A. Alkhateeb, A. K. Gupta, and R. W. Heath, Jr., "Modeling and analyzing millimeter wave cellular systems," *IEEE Trans. Commun.*, vol. 65, no. 1, pp. 403–430, Jan. 2017.

[18] M. D. Renzo, "Stochastic geometry modeling and performance evaluation of mmwave cellular communications," in *Proc. IEEE Int. Conf. Commun. (ICC)*, Jun. 2015, pp. 5992–5997.

[19] T. Bai and R. W. Heath, Jr., "Coverage and rate analysis for millimeter-wave cellular networks," *IEEE Trans. Wireless Commun.*, vol. 14, no. 2, pp. 1100–1114, Feb. 2015.

[20] E. Turgut and M. C. Gursoy, "Coverage in heterogeneous downlink millimeter wave cellular networks," *IEEE Trans. Commun.*, vol. 65, no. 10, pp. 4463–4477, Oct. 2017.

[21] S. Singh, M. N. Kulkarni, A. Ghosh, and J. G. Andrews, "Tractable model for rate in self-backhauled millimeter wave cellular networks," *IEEE J. Sel. Areas Commun.*, vol. 33, no. 10, pp. 2196–2211, Oct. 2015.

[22] D. Maamari, N. Devroye, and D. Tuninetti, "Coverage in mmWave cellular networks with base station co-operation," *IEEE Trans. Wireless Commun.*, vol. 15, no. 4, pp. 2981–2994, Apr. 2016.
[23] H. He, J. Xue, T. Ratnarajah, and M. Sellathurai, "Performance analysis of millimeter wave cloud radio access networks," in *Proc. IEEE Global Commun. Conf. (GLOBECOM)*, Dec. 2016, pp. 1–6.
[24] X. Zhang and J. G. Andrews, "Downlink cellular network analysis with multi-slope path loss models," *IEEE Trans. Commun.*, vol. 63, no. 5, pp. 1881–1894, May 2015.
[25] S. Buzzi and C. D'Andrea, "User-centric communications versus cell-free massive MIMO for 5G cellular networks," in *Proc. 21st Int. ITG Workshop Smart Antennas*, Mar. 2017, pp. 1–6.
[26] T. Bai, R. Vaze, and R. W. Heath, Jr., "Analysis of blockage effects on urban cellular networks," *IEEE Trans. Wireless Commun.*, vol. 13, no. 9, pp. 5070–5083, Sep. 2014.
[27] Y. Lin and W. Yu, "Downlink spectral efficiency of distributed antenna systems under a stochastic model," *IEEE Trans. Wireless Commun.*, vol. 13, no. 12, pp. 6891–6902, Dec. 2014.
[28] D. Moltchanov, "Distance distributions in random networks," *Ad Hoc Netw.*, vol. 10, no. 6, pp. 1146–1166, 2012.
[29] F. Baccelli, B. Blaszczyszyn, and P. Muhlethaler, "Stochastic analysis of spatial and opportunistic aloha," *IEEE J. Sel. Areas Commun.*, vol. 27, no. 7, pp. 1105–1119, Sep. 2009.
[30] S. G. Krantz, *Real Analysis and Foundations*. London, U.K.: Chapman & Hall, 2004.
[31] O. Onireti, A. Imran, and M. A. Imran, "Coverage, capacity, and energy efficiency analysis in the uplink of mmWave cellular networks," *IEEE Trans. Veh. Technol.*, vol. 67, no. 5, pp. 3982–3997, May 2018.
[32] F. Baccelli and B. Blaszczyszyn, *Stochastic Geometry and Wireless Networks: Theory*. Boston, MA, USA: Now, 2009, nos. 1–2.
[33] K. A. Hamdi, "Capacity of MRC on correlated rician fading channels," *IEEE Trans. Commun.*, vol. 56, no. 5, pp. 708–711, May 2008.

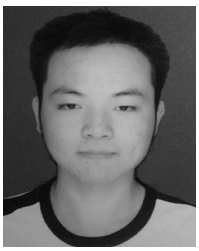

JIANFENG SHI received the B.S. degree in communication engineering from Nanjing Normal University, Nanjing, China, in 2014. He is currently pursuing the Ph.D. degree with the National Mobile Communication Research Laboratory, Southeast University. From 2017 to 2018, he was a Visiting Student with the Department of Electrical Computer Engineering, McGill University, Canada. His research interests include D2D communication, user-centric networks, and dynamic optimization. He served as a TPC Member for the IEEE ICC, WCNC, and CIC ICCC, from 2015 to 2018.

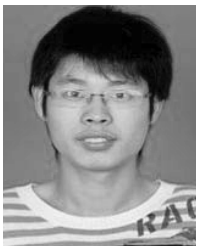

CUNHUA PAN received the B.S. and Ph.D. degrees from the School of Information Science and Engineering, Southeast University, Nanjing, China, in 2010 and 2015, respectively. From 2015 to 2016, he was a Research Associate with the University of Kent, U.K. He holds the Postdoctoral position with the Queen Mary University of London, U.K. His research interests mainly include ultra-dense C-RAN, machine learning, UAV, the Internet of Things (IoT), and mobile edge computing. He serves as an Editor for the IEEE ACCESS, the Student Travel Grant Chair for ICC 2019, and a TPC Member for numerous conferences, such as ICC and GLOBECOM.

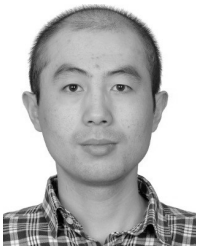

WENCE ZHANG received the Ph.D. degree from the National Mobile Communications Research Laboratory, Southeast University, China, in 2015. From 2013 to 2014, he was a Visiting Student with the Department of Electronics, University of York, U.K. From 2015 to 2016, he was a Postdoctoral Researcher with CETUC, PUC-Rio, Brazil. Since 2016, he has been a Lecturer with Jiangsu University, China. His research interests include distribute antenna systems and massive MIMO. He served as a TPC Member for the IEEE ICC 2015-2017 and a Session Chair for the IEEE SAM 2016.

MING CHEN received the B.Sc., M.Sc., and Ph.D. degrees in mathematics from Nanjing University, Nanjing, China, in 1990, 1993, and 1996, respectively. In 1996, he joined the National Mobile Communications Research Laboratory, Southeast University, as a Lecturer. From 1998 to 2003, he was an Associate Professor and since 2003, and he has been a Professor with the Laboratory. His research interests include signal processing and radio resource management of mobile communication systems.